RSC Advances

PAPER

Cite this: *RSC Adv.*, 2020, **10**, 17094

Nanocomposite liposomes for pH-controlled porphyrin release into human prostate cancer cells†

German V. Fuentes,[a] Eric N. Doucet,[a] Alyson Abraham,[a] Nikki K. Rodgers,[a] Felix Alonso,[a] Nelson Euceda,[a] Michael H. Quinones,[a] Penelope A. Riascos,[a] Kristelle Pierre,[b] Nuhash H. Sarker,[b] Manya Dhar-Mascareno,*[bd] Mircea Cotlet,[c] Kim Kisslinger,[c] Fernando Camino,[c] Mingxing Li,[c] Fang Lu[c] and Ruomei Gao *[ad]

It is both challenging and desirable to have drug sensitizers released at acidic tumor pH for photodynamic therapy in cancer treatment. A pH-responsive carrier was prepared, in which fumed silica-attached 5,10,15,20-tetrakis(4-trimethylammoniophenyl)porphyrin (TTMAPP) was encapsulated into 1,2-dioleoyl-*sn*-glycero-3-phosphocholine (DOPC) nanocomposite liposomes. The sizes of agglomerates were determined by dynamic light scattering to be 115 nm for silica and 295 nm for silica-TTMAPP-DOPC liposomes. Morphological changes were also found in TEM images, showing liposome formation at pH 8.5 but collapse upon silanol protonation. TTMAPP release is enhanced from 13% at pH 7.5 to 80% at pH 2.3, as determined spectrophotometrically through dialysis membranes. Fluorescence emission of TTMAPP encapsulated in the dry film of liposomes was reduced to half at pH 8.6 when compared to that at pH 5.4, while the production of singlet oxygen was quintupled at pH 5.0 compared to pH 7.6. Upon treatment of human prostate cancer cells with liposomes containing 6.7 μM, 13 μM, 17 μM and 20 μM TTMAPP, the cell viabilities were determined to be 60%, 18%, 20% and 5% at pH 5.4; 58%, 30%, 25% and 10% at pH 6.3; and 90%, 82%, 68% and 35% at pH 7.4, respectively. Light-induced apoptosis in cancerous cells was only observed in the presence of liposomes at pH 6.3 and pH 5.4 but not at pH 7.4, as indicated by chromatin condensation.

Received 28th January 2020
Accepted 21st April 2020

DOI: 10.1039/d0ra00846j

rsc.li/rsc-advances

Introduction

Developing a drug carrier that is capable of releasing medication at acidic pH, as found in the sites of tumor growth,[1,2] is beneficial but challenging.[3] Smart nanocarriers[4] have been actively investigated for this purpose, in which porous inorganic supports are used for cargo loading and functional gated materials for cargo sealing and release.[5] Among those delivery systems, there are few using a built-in trigger (*e.g.*, photothermal core stimulator of gold nanoparticles[6–8]) to stimulate carrier disassembly. Such a strategy greatly expands the choice of gated materials and has yet to be developed in terms of easy preparation, desirable biocompatibility and acidic sensitivity.

Unlike the widespread applications of mesoporous silica nanoparticles as a direct pH-trigger,[9–13] a protective shell for liposomes,[14,15] and a support for lipid layers,[16–19] much less is known about the properties of fumed silica for nanomedicines. Thermally treated fumed silica is a voluminous powder composed of aggregates, which cluster into three-dimensional branched networks called agglomerates.[20,21] Their wide variation in cross linked holes and strong affinity of numerous silanols[22] for hydrogen bonding make them a promising drug carrier through various interfacial mechanisms. Gomes and coworkers found that the Si-MCM-41 samples synthesized with fumed silica presented better adsorption performance than those synthesized with tetraethyl orthosilicate.[23] A recent study showed that a porphyrin array coated with amorphous silica allowed the efficient production of singlet oxygen ($^1O_2$),[24] a reactive oxygen species used in the dosimetry of photodynamic therapy (PDT).[25] Fumed silica has been widely used as food additives for decades.[26,27] The United States Food and Drug Administration (FDA) allows an addition up to 2% silica by weight of food.[27] In recent years, there are a number of studies

[a]*Chemistry and Physics Department, State University of New York College at Old Westbury, Old Westbury, New York 11568, USA. E-mail: gaor@oldwestbury.edu*
[b]*Biological Sciences Department, State University of New York College at Old Westbury, Old Westbury, New York 11568, USA. E-mail: mascarenom@oldwestbury.edu*
[c]*Center for Functional Nanomaterials, Brookhaven National Laboratory, Upton, NY 11973, USA*
[d]*Institute for Cancer Research and Education, State University of New York College at Old Westbury, Old Westbury, NY 11568, USA*

† Electronic supplementary information (ESI) available: Determinations of molar ratio of TTMAPP over silica, extinction coefficients of TTMAPP, liposome stability, additional TEM images, quantum yield of singlet oxygen production, dark controls of cytotoxicity and DAPI staining assay at different pH. See DOI: 10.1039/d0ra00846j

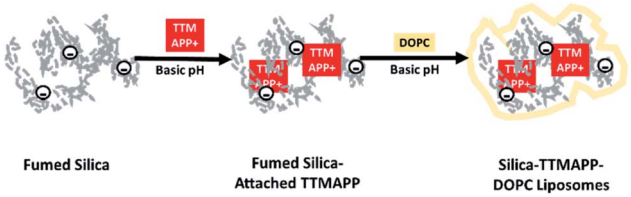

Scheme 1 Formation of silica-TTMAPP-DOPC.

indicating the toxicity of fumed silica through the formation of reactive oxygen species,[28] the accumulation in rats' spleen,[29] *etc.* This topic is currently under discussion in terms of dose-dependence, risk research and regulatory decisions.[30]

The work presented herein uses fumed silica cores to stimulate drug release from liposomes. A cationic $^1O_2$ sensitizer, 5,10,15,20-tetrakis(4-trimethylammoniophenyl)porphyrin (TTMAPP), adsorbed onto anionic silica surface at basic pH through electrostatic attraction. This silica–TTMAPP complex was then fused with 1,2-dioleoyl-*sn-glycero*-3-phosphocholine (DOPC) to form nanocomposite liposomes (silica-TTMAPP-DOPC in Scheme 1). Upon the protonation of silanol groups at weak acidic pH, negative discharge occurs on the silica surface,[31] thus leading to TTMAPP desorption and liposome collapse. This paper reports the preparation and characterization of silica-TTMAPP-DOPC as well as initial evaluation of therapeutic effectiveness in treating human prostate cancer cells.

Experimental section

Materials and instruments

Fumed silica powders (primary particle size = 7 nm, density = 2.3 lb per ft^3) were purchased from Sigma-Aldrich. Tetrakis(4-trimethylammoniophenyl)porphyrin tetrachloride or tetra(*p*-toluenesulfonate) (TTMAPP), and *meso*-tetrakis(*p*-sulfonatophenyl) porphyrin (TSPP) were purchased from Frontier Scientific, Inc. or Sigma-Aldrich. 4-(2-Hydroxyethyl)-1-piperazineethanesulfonic acid (HEPES), deuterium oxide and 1,2-dioleoyl-*sn-glycero*-3-phosphocholine (DOPC) were purchased from Fisher Scientific. All chemicals were obtained with the highest grades available. Human prostate cancer cell line, DU145, was purchased from ATCC (Manassas, VA). Cell Counting Kit-8 (CCK-8) was purchased from Dojindo Molecular Technologies. A Thermo Scientific Evolution 220 UV-visible spectrophotometer was used for measuring light absorbed. A scanning confocal fluorescence lifetime imaging microscope based on an inverted Olympus IX81 frame (100×, 0.95NA Olympus dry lens) was used to record fluorescence lifetime and intensity images upon optical excitation at 410 nm resulted from a frequency doubled Ti:sapphire laser (Spectra Physics Maitai) with 85 fs pulses of 8 MHz repetition rate [with the help of a 560 nm dichroic (Semrock) and a 600 nm long pass filter (Semrock)]. The detailed instrument setup can be found from our previous work.[32] A Q-switched Nd:YAG laser with a pulse duration of 3–4 ns and a maximum energy of 30 mJ at 532 nm (Polaris II-20, New Wave Research Merchantek Products) and a repetition rate of 20 Hz in combination with a FT 200 Fluorimeter (Picoquant) equipped with an InGaAs Hamamatsu micro channel photomultiplier were used for time-resolved $^1O_2$ luminescence measurements. The luminescence decay of $^1O_2$ at 1270 nm was monitored at the right angle. Time-resolved data were fit using the Fluofit Picoquant software. A JEM-1400 Transmission Electron Microscope (TEM) from JEOL USA, Inc. and 200 Mesh Copper TEM grids from TED PELLA, Inc. were used for particle characterization. A Malvern Zetasizer (Nano Series) was used for dynamic light scattering (DLS) analysis of particle sizes and distributions. An AccuTherm Microtube Shaking Incubator from Labnet International, Inc. and an ultrasonic bath from Fisher Scientific, Inc. were used for liposome preparation. The irradiation light power was determined by Newport Optical Power Meter (1916-C). All experiments were carried out at ambient temperature.

Preparation of colloidal silica solution

The colloidal silica was prepared by dispersing 1.0 g fumed silica powers in 500 mL pH 9–10 NaOH solution, followed by stirring for days under basic pH and filtering with the double layers of Whatman qualitative filter paper (Grade 4). Its concentration is reported in terms of primary particles (C_{SiO_2}, M) with an estimated diameter of 7 nm and silica density of d_{SiO_2} = 2.3 g cm^{-3} to better reflect experimental conditions (eqn (1)). This silica stock solution has a particle concentration around 8×10^{-6} M.

$$C_{SiO_2}, M = \frac{\dfrac{C_{SiO_2},\ \mathrm{g\ L^{-1}}}{d_{SiO_2},\ \mathrm{g\ cm^{-3}}}}{\dfrac{4}{3}\pi\left(\dfrac{\phi_{SiO_2},\ \mathrm{nm}}{2} \times 1 \times 10^{-7}\right)^3 \times 6.02 \times 10^{23}} \quad (1)$$

Preparation of silica-attached TTMAPP

An aliquot of 1.00 mL 2.0×10^{-4} M aqueous TTMAPP solution was added into 4.00 mL of stock silica solution. The mixture was stirred for *ca.* 30 minutes. The silica-attached TTMAPP nanoparticles were then separated from free TTMAPP in solution by centrifugation, followed by re-dispersing in 10.00 mL of pH 9 NaOH or 0.05 M pH 7.4 HEPES buffer solutions.

Preparation of silica-TTMAPP-DOPC nanocomposite liposomes

Liposomes were prepared by lipid film hydration. Briefly, 0.03 g DOPC was thoroughly dissolved in 1 mL chloroform in a 20 mL glass vial that was then placed in a vacuum desiccator overnight to yield a dry lipid film. The DOPC film was stored frozen until ready to hydrate. 10 mL of silica-attached TTMAPP in pH 9 NaOH solution or 0.01 M pH 7.4 HEPES buffer solution was added into the dry lipid film. The mixture was shaken at room temperature under 700 revolutions per minute for up to 1 hour, and then sonicated until a homogeneous dispersion was obtained. The prepared liposomes were precipitated by centrifugation and re-dispersed in NaOH or HEPES buffer solutions as needed to remove any free TTMAPP in the solution.

Production of $^1O_2$ and its quantum yield

The generation of $^1O_2$ was observed directly at its 1270 nm emission upon irradiation of desorbed TTMAPP at 532 nm in D_2O. The kinetic fitting of $^1O_2$ decay was obtained using FluoFit software. The quantum yield of $^1O_2$ production (ϕ_Δ) by TTMAPP was determined using previously established methods[10] and calculated according to eqn (2). The absorbance of TTMAPP samples and a reference of TSPP with a known quantum yield of 0.63 (ref. 33) was controlled between 0.01 and 0.8 at an excitation wavelength of 532 nm. The initial $^1O_2$ intensities were extrapolated to time zero for each measurement. The data points from the initial few ns were not used due to interfering signals from more rapid events coincident with the laser pulse (*e.g.*, scattered light, electronic interference of the detector, *etc.*).

$$\frac{\phi_{\Delta,\mathrm{TTMAPP}}}{\phi_{\Delta,\mathrm{TSPP}}} = \frac{\mathrm{slope}_{\mathrm{TTMAPP}}}{\mathrm{slope}_{\mathrm{TSPP}}} \quad (2)$$

Here $\phi_{\Delta,\mathrm{TTMAPP}}$ and $\phi_{\Delta,\mathrm{TSPP}}$ are ϕ_Δ from TTMAPP sample and TSPP reference, respectively. $\mathrm{Slope}_{\mathrm{TTMAPP}}$ and $\mathrm{slope}_{\mathrm{TSPP}}$ represent the slopes derived from linear response of $^1O_2$ signals as a functional of absorbance at 532 nm for TTMAPP and TSPP, respectively (Fig. S1 in ESI†).

pH-controlled porphyrin release and liposome stability

A 10 mL aliquot of nanocomposite liposomes was transferred into pre-hydrated dialysis tubing. The dialysis membrane was mechanically sealed and placed into a beaker containing 1 L of deionized water at different pH ranging from 2 to 9 adjusted by adding an appropriate amount of NaOH or HCl. For the TTMAPP release test, samples of 3.00 mL dialysates at different pH were taken after 5 hours of dialysis (Fig. 3). For liposome stability test, samples of 3.00 mL dialysates were taken at an interval of two or more hours for up to a timespan of 60 hours (Fig. S2 in ESI†). The pH of each 3.00 mL of dialysate was then adjusted to be the same for TTMAPP analysis spectrophotometrically at 412 nm using an extinction coefficient of 3.6×10^5 M^{-1} cm^{-1} (Fig. S3 in ESI†).

Cell culture

DU145 cells were cultured in RPMI 1640 medium supplemented with penicillin/(100 U mL^{-1}) streptomycin 10 μg mL^{-1} and 10% heat inactivated fetal calf serum cells at 37 °C in a humidified atmosphere containing 5% CO_2. Cells were plated on 96 well plate at 1×10^4 cells per well. On the next day cells were changed to serum-free RPMI 1640 medium and processed for treatment with silica-TTMAPP-DOPC at different pH.

Treatment

Complete medium from the cells was replaced with serum-free medium. Two sets of DU145 cells on 96 well plates were exposed to different doses of silica-TTMAPP-DOPC and corresponding control solutions containing the same amounts of silica and DOPC in the absence of TTMAPP at pH 5.4, pH 6.3 and pH 7.4, respectively, respectively. One set was irradiated at 250–600 nm with an average power of 8.7 mW for 60 minutes. Another set was kept under darkness. The cells were then placed in the cell incubator for 3 hours.

Cell viability assay

The cell viability was evaluated by CCK-8 assay. The medium was aspirated out of the wells and replaced with 100 μL medium containing CCK-8 and incubated for an additional 3 hours. The absorbance was taken at 450 nm against untreated cells using a microplate reader (VICTORX3 PerkinElmer). Percent viability was calculated as

$$\frac{\text{Absorbance of sample}}{\text{Absorbance of control}} \times 100.$$

For statistical analysis, comparisons between the groups were performed using one-way analysis of variance (ANOVA). Differences between means of different treatments were inspected with Bonferroni multiple comparison *post hoc* tests. The data were analyzed using GraphPad Prism (GraphPad Software La Jolla, CA, USA). P values of <0.05, <0.01, and <0.001 were considered as statistically significant.

DAPI staining for apoptosis

DU145 cells (5×10^4 cells per well) were grown in 6 well-plates on a glass cover slip and treated with liposomes containing 13 μM TTMAPP at pH 5.4, pH 6.3 and pH 7.4. The treated cells were washed with PBS and fixed in 3.8% formaldehyde for 15 min. Cells were then stained with 4′,6-diamidino-2-phenylindole (DAPI, 1 μg mL^{-1}) in PBS at 37 °C for 30 min, followed by fluorescence microscopy analysis.

Results and discussion

Formation of nanocomposite liposomes

The biocompatibility and encapsulating capability make liposomes a promising carrier for both hydrophobic and hydrophilic drugs.[34] With isoelectric point values between pH 2 and 4,[31] fumed silica particles are ready to attach to cationic TTMAPP molecules *via* electrostatic attraction in weak basic solutions. This silica-attached TTMAPP complex was then fused with DOPC to form nanocomposite silica-TTMAPP-DOPC liposomes. The morphology of silica-TTMAPP-DOPC was examined by TEM at different pH. Fig. 1 shows that lipid layers are visible at pH 8.5 due to the formation of amorphous liposomes (image A). The variation of pH changes the protonation of silanol

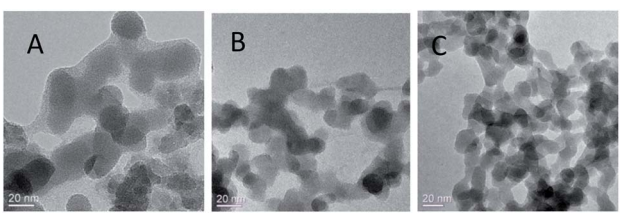

Fig. 1 TEM images of silica-TTMAPP-DOPC at pH 8.5 (A), 5.0 (B) and 2.0 (C).

groups, thus the charge and morphology of nanocomposite liposomes. The sizes of primary particles in silica-TTMAPP-DOPC decreased from *ca.* 25 nm at pH 8.5 (image A) to *ca.* 15 nm at pH 5.0 (image B) to *ca.* 10 nm at pH 2.0 (image C), which is comparable to commercially reported value of 7 nm for primary fumed silica particles. Additional TEM images of silica-TTMAPP-DOPC at basic pH can be found in Fig. S4 in ESI.† The diameters of agglomerates were also determined by dynamic light scattering (DLS) to have increased from 115 nm for silica colloids to 295 nm for liposomes (Fig. 2). For easy characterization, silica particle concentrations were calculated using its primary size although the actual framework is much larger due to the formation of amorphous agglomerates. The number of TTMAPP molecules adsorbed onto each primary silica particle was estimated to be 4.5 by examining the ratios of TTMAPP to silica particles at pH 9 (Fig. S1 in ESI†).

Effect of pH on TTMAPP release

The nature of the permeability barrier in the membranes still remains unclear, especially with respect to ionic solutes. It has long been known that proton leakage through lipid membranes takes place even in the absence of channels, and its transport proceeds up to several orders of magnitude faster than that of other small cations.[35] To reveal the process of pH-triggered collapse of nanocomposite liposomes, the amount of TTMAPP passing through the dialysis tubing was monitored spectrophotometrically as a function of pH through the course of 5 hour-dialysis, using an extinction coefficient of $3.6 \times 10^5\ M^{-1}\ cm^{-1}$ for TTMAPP (Table S1 and Fig. S2 in ESI†). The initial pH of liposomes was controlled to be 7.4 while the pH of dialysates varying between 2 and 9. As illustrated in Fig. 3, TTMAPP release from liposomes is negligible at pH 8–9 (~10%) and pH 7.5 (~13%) but is dramatically accelerated up to 38% at pH 6.0, 49% at pH 5.2, 53% at pH 4.8, 66% at pH 3.3 and 80% at pH 2.3, indicating a pH-responsive porphyrin release and proton permeability across the imperfect lipid layers. The pores formed with lipid head groups have been suggested to be responsible for the passage of ions and polar molecules across membranes.[36] Moreover, our stability test reveals a complete liposome collapse in 35 hours at pH 7.5 but 15 hours at pH 5.6, indicating an optimum endurance of silica-TTMAPP-DOPC in basic solution (Fig. S3 in ESI†). With TTMAPP released by 13%

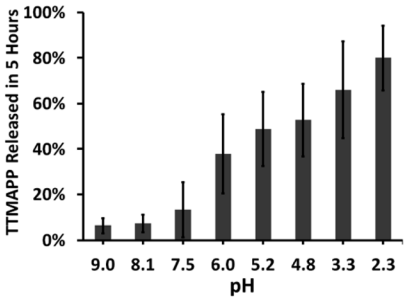

Fig. 3 Effect of pH on the release of TTMAPP from liposomes after 5 hours of dialysis ($n = 2$–6).

at pH 7.5 and 80% at pH 2.3, our results also indicated a limitation toward specificity and effectiveness. Its physiological efficacy would be even harder to be evaluated. A promising alterative for active target is to use nano-carriers modified with specific cancer target receptors, such as antibodies,[37,38] folates,[38] *etc.* This strategy could also be applied to silica-liposome carriers for further improvement of drug delivery.

The pH-dependent TTMAPP release was also confirmed by $^1O_2$ production (Fig. 4) and TTMAPP fluorescence images as well as its kinetic decays obtained from liposome dry layers (Fig. 5). The quantum yield of $^1O_2$ production upon irradiation of TTMAPP at 532 nm was determined to be 0.76 in D_2O using TSPP as a reference (Fig. S5 in ESI†),[33] which is consistent with the literature report.[39] The pH-controlled photosensitization of TTMAPP is shown in Fig. 4, in which $^1O_2$ production at pH 5.0 (black line) is ~5-fold higher than that at pH 7.6 (green line). The efficient quenching of $^1O_2$ emission was observed in the presence of NaN_3 (red line), a trap of $^1O_2$ with 2nd order quenching rate constant over 8 orders of magnitude.[40] Fig. 4 shows that the azide ions reduce not only the lifetime of $^1O_2$ but also its initial intensity, which can be explained by its reactions with both $^1O_2$ and excited states of the sensitizer.[41] The lifetime of $^1O_2$ depends largely on its surroundings. A lifetime of 30 μs was obtained under our experimental conditions, which is shorter than that determined in pure D_2O (*e.g.*, 53 μs (ref. 42)) but acceptable if considering the complex experimental media.

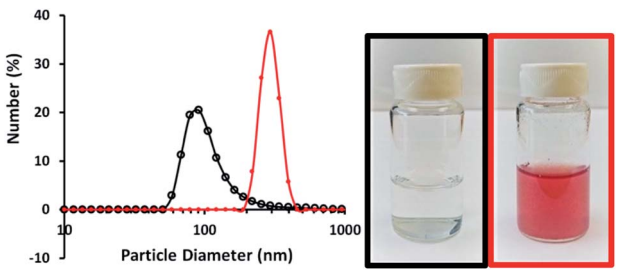

Fig. 2 Dynamic light scattering of silica colloids with a diameter of 115 nm (black line and picture in black frame) and silica-TTMAPP-DOPC with a diameter of 295 nm (red line and picture in red frame) in pH 9 NaOH solutions.

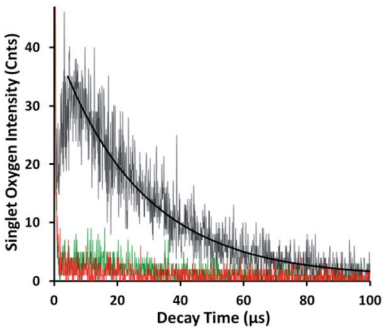

Fig. 4 Emission of $^1O_2$ at 1270 nm upon irradiation (532 nm) of released TTMAPP at pH 7.6 (green line), pH 5.0 in the absence (black line) and presence (red line) of 1 mM NaN_3.

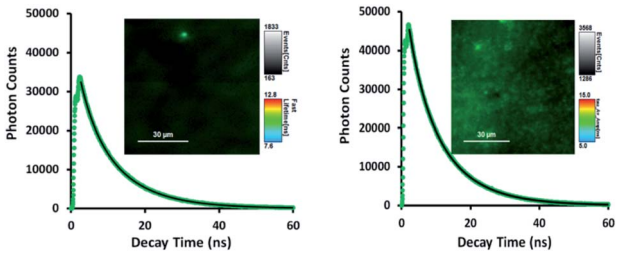

Fig. 5 Representative fluorescence decays and lifetime images monitored at 560 nm upon irradiation (410 nm) of TTMAPP in the dry layers of liposomes at pH 8.6 (left) and pH 5.4 (right), dashed green lines – experimental data, and solid black lines – 1st-order kinetic fitting.

As shown in Fig. 5, TTMAPP fluorescence lifetimes calculated by 1st-order kinetic fitting at pH 5.4 and pH 8.6 remained unchanged with an average of 9.5 ns for pH 8.6 (left decay) and 9.6 ns for pH 5.4 (right decay). However, a noticeable reduction of initial intensity at basic pH (left decay and image) suggests that TTMAPP molecules were encapsulated inside liposomes. The coverage of DOPC layers over silica-attached TTMAPP at pH 8.6 acted as a neutral filter that to some extent hampered TTMAPP from the absorption of excitation light, thus leading to a lower initial intensity on the decay curve and a darker image of fluorescence. The emission nearly doubled as pH dropped from pH 8.6 (cnts = 1833, left image) to pH 5.4 (cnts = 3568, right image). In the acidic environment, released TTMAPP absorbs excitation light efficiently, leading to a strong emission (right image) and effective production of $^1O_2$ (Fig. 4).

Cytotoxic effect of silica-TTMAPP-DOPC on human prostate cancer cells

It is well known that light-activated photosensitizing reagents cause oxidative stress and tumor cell death by producing reactive oxygen species, especially $^1O_2$.[25] Enhanced apoptotic effects upon phthalocyanine photosensitization were also observed.[43] To mimic the acidic environment in tumor cells, silica-TTMAPP-DOPC was adjusted to weak acidic pH and the toxicity was evaluated in DU145, a human prostate cancer cell line (Fig. 6A). Cells were exposed to silica-TTMAPP-DOPC at pH 5.4, 6.3 and 7.4 under light irradiation as well as in darkness, and control treatments were done for silica–DOPC in the absence of TTMAPP. Loss of cell viability was negligible when exposed to light in the presence of silica–DOPC controls at all pH (red, blue and black dash lines for pH 5.4, pH 6.3 and pH 7.4, respectively). However, reduced cell viability was observed in the presence of silica-TTMAPP-DOPC in a TTMAPP-concentration-dependent manner, as determined to be 60%, 18%, 20% and 5% at pH 5.4 (solid red line); 58%, 30%, 25% and 10% at pH 6.3 (solid blue line); and 90%, 82%, 68% and 35% at pH 7.4 (solid black line) when treated with liposomes containing 6.7 μM, 13 μM, 17 μM and 20 μM TTMAPP, respectively. Although reduced cell viability (35%) was observed in the presence of 20 μM TTMAPP at pH 7.4, it was seven-fold higher than that at pH 5.4 (5%). A significant difference was found for

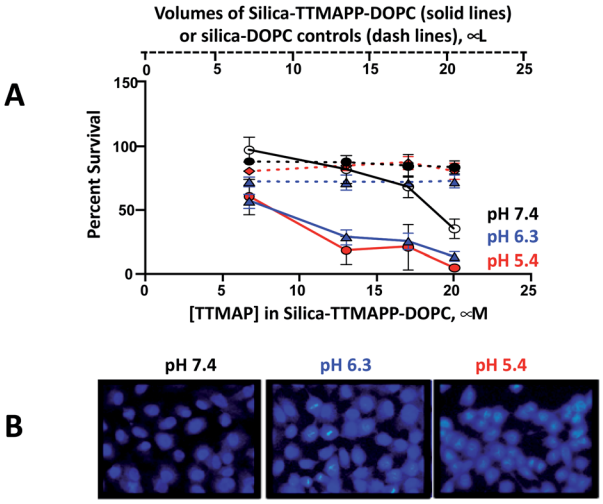

Fig. 6 (A) Light-induced cytotoxicity of silica-TTMAPP-DOPC on DU145 cells incubated at pH 7.4 (solid black lines), pH 6.3 (solid blue line) and pH 5.4 (solid red line) as a function of TTMAPP concentrations. The corresponding colored dash lines represent controls with same amount of silica and DOPC in the absence of TTMAPP. The data represents the plot of mean cell viability ± standard deviation with n = 4. (B) Detection of DU145 cell death by DAPI staining assay upon cell treatments with silica-TTMAP-DOPC containing 13 μM TTMAPP at pH 7.4, pH 6.3 and pH 5.4. Representative fields out of six fields are shown here.

silica-TTMAPP-DOPC between pH 7.4 and pH 5.4, as well as between pH 7.4 and pH 6.3 ($P < 0.001$), and between silica-TTMAPP-DOPC and silica–DOPC controls at pH 5.4 and at pH 6.3 ($P < 0.001$); while there was no difference in cell viability at pH 7.4 between silica-TTMAPP-DOPC and silica–DOPC controls for all TTMAPP concentrations ($P > 0.05$) except for the highest one of 20 μM ($P < 0.001$). A loss of cell viability was not seen with dark controls under all conditions above (Fig. S6 in ESI†). These observations are consistent with pH-responsive TTMAPP release and liposome collapse. It is known that apoptosis results in specific and stage-dependent morphological alterations of the cell nucleus. Chromatin condensation is typical of apoptotic cells and often precedes nuclear fragmentation. DU145 cells were stained with DAPI and treated with liposomes containing 13 μM TTMAPP. The assessment of nuclear morphology by fluorescence microscopy was performed using cell-permeable nucleic acid stains, such as DAPI.[44] As shown in the photomicrographs in Fig. 6B the nuclear chromatin condensation was only observed in photo-activated drug treated cells at pH 5.4 and 6.3 but not at pH 7.4. The number of nuclei in the field were counted displaying nuclear fragmentation, chromatin condensation, or nuclear condensation (Fig. S7†).

Conclusions

A simple fabrication method was developed to encapsulate fumed silica-attached porphyrin into liposomes composed of DOPC. The nanocomposite liposomes prepared are relatively stable in weak basic solutions but effectively release porphyrins for $^1O_2$ production at acidic pH for PDT in cancer treatment.

The potential application of this nanoplatform is indicated by the pH-controlled sensitizer release, decreased fluorescence of encapsulated TTMAPP, quintupled $^1O_2$ phosphorescence and efficient loss of cell viability at tumor pH. An incorporation of internal silica trigger with lipid layers not only greatly extends the selection of lipids but also provides a function of lipid modification for future targeting and detection.

Conflicts of interest

There are no conflicts to declare.

Acknowledgements

We thank the support from Chemistry and Physics Department, Biological Sciences Department, Faculty Development Grants at SUNY Old Westbury. This research used resources of the Center for Functional Nanomaterials, which is a U.S. DOE Office of Science Facility, at Brookhaven National Laboratory under Contract No. DE-SC0012704. The work is also partially supported by NSF-IUSE (1611887), NIH (R15CA169984), NYSED-CSTEP (C402579), NYSED-STEP (C402605) and NYS DOH01-C30319GG at SUNY Old Westbury. Authors also thank Professor Judith Lloyd at SUNY Old Westbury for helpful discussions.

References

1 L. E. Gerweck, *Semin. Radiat. Oncol.*, 1998, **8**, 176–182.
2 H. Gabriel, A. Sckell, M. Dellian, N. S. Forbes and R. K. Jain, *Clin. Cancer Res.*, 2002, **8**, 1284–1291.
3 M. Kanamala, W. R. Wilson, M. Yang, B. D. Palmer and Z. Wu, *Biomaterials*, 2016, **85**, 152–167.
4 D. Peer, J. M. Karp, S. Hong, O. C. Farokhzad, R. Margalit and R. Langer, *Nat. Nanotechnol.*, 2007, **2**, 751–760.
5 E. Aznar, M. Oroval, L. Pascual, J. R. Murguía, R. Martínez-Máñez and F. Sancenón, *Chem. Rev.*, 2016, **116**, 561–718.
6 M. Adeli, R. S. Sarabi, R. Yadollahi Farsi, M. Mahmoudi and M. Kalantari, *J. Mater. Chem.*, 2011, **21**, 18686–18695.
7 A. Barhoumi, W. Wang, D. Zurakowski, R. S. Langer and D. S. Kohane, *Nano Lett.*, 2014, **14**, 3697–3701.
8 S. Bhana, G. Lin, L. Wang, H. Starring, S. R. Mishra, G. Liu and X. Huang, *ACS Appl. Mater. Interfaces*, 2015, **7**, 11637–11647.
9 K.-N. Yang, C.-Q. Zhang, W. Wang, P. C. Wang, J.-P. Zhou and X.-J. Liang, *Cancer Biol. Med.*, 2014, **11**, 34–43.
10 W. Li, W. Lu, Z. Fan, X. Zhu, A. Reed, B. Newton, Y. Zhang, S. Courtney, P. T. Tiyyagura, R. R. Ratcliff, S. Li, E. Butler, H. Yu, P. C. Ray and R. Gao, *J. Mater. Chem.*, 2012, **22**, 12701–12708.
11 H. Zheng, C.-W. Tai, J. Su, X. Zou and F. Gao, *Dalton Trans.*, 2015, **44**, 20186–20192.
12 T. Yan, J. Cheng, Z. Liu, F. Cheng, X. Wei and J. He, *Colloids Surf., B*, 2018, **161**, 442–448.
13 Y. Chen, K. Ai, J. Liu, G. Sun, Y. Qi and L. Lu, *Biomaterials*, 2015, **60**, 111–120.
14 N. Folliet, C. Roiland, S. Begu, A. Aubert, T. Mineva, A. Goursot, K. Selvaraj, L. Duma, F. Tielens, F. Mauri, G. Laurent, C. Bonhomme, C. Gervais, F. Babonneau and T. Azaïs, *J. Am. Chem. Soc.*, 2011, **133**, 16815–16827.
15 S. Shen, L. Yang, Y. Lu, J.-G. Chen, S. Song, D. Hu and A. Parikh, *ACS Appl. Mater. Interfaces*, 2015, **7**, 25039–25044.
16 J. Liu, X. Jiang, C. Ashley and C. J. Brinker, *J. Am. Chem. Soc.*, 2009, **131**, 7567–7569.
17 J. Liu, A. Stace-Naughton, X. Jiang and C. J. Brinker, *J. Am. Chem. Soc.*, 2009, **131**, 1354–1355.
18 A. E. LaBauve, T. E. Rinker, A. Noureddine, R. E. Serda, J. Y. Howe, M. B. Sherman, A. Rasley, C. J. Brinker, D. Y. Sasaki and O. A. Negrete, *Sci. Rep.*, 2018, **8**, 13990.
19 V. Colapicchioni, S. Palchetti, D. Pozzi, E. S. Marini, A. Riccioli, E. Ziparo, M. Papi, H. Amenitsch and G. Caracciolo, *J. Mater. Chem. B*, 2015, **3**, 7408–7416.
20 H. Barthel, L. Rösch and J. Weis, in *Organosilicon Chemistry Set*, Wiley-VCH Verlag GmbH, 2008, pp. 761–778, DOI: 10.1002/9783527620777.ch91a.
21 A. Bogdan, in *Encyclopedia of Surface and Colloid Science*, ed. P. Somasundaran, CRC Press, Taylor & Francis Group, Boca Raton, FL, 2nd edn, 2006, vol. 2.
22 C. C. Liu and G. E. Maciel, *J. Am. Chem. Soc.*, 1996, **118**, 5103–5119.
23 G. A. Assumpção, J. G. R. Poço, R. Fernández-Felisbino, D. Cardoso and E. L. Gomes, *Adsorpt. Sci. Technol.*, 2015, **33**, 203–221.
24 J. Wang, Y. Zhong, X. Wang, W. Yang, F. Bai, B. Zhang, L. Alarid, K. Bian and H. Fan, *Nano Lett.*, 2017, **17**, 6916–6921.
25 M. T. Jarvi, M. J. Niedre, M. S. Patterson and B. C. Wilson, *Photochem. Photobiol.*, 2006, **82**, 1198–1210.
26 E. F. S. A. (EFSA), *EFSA J.*, 2009, **1132**, 1–24.
27 U. S. F. D. Administration, *Sec. 172.480 Silicon dioxide*, https://www.accessdata.fda.gov/scripts/cdrh/cfdocs/cfCFR/CFRSearch.cfm?fr=172.480, accessed March, 2020.
28 H. Zhang, D. R. Dunphy, X. Jiang, H. Meng, B. Sun, D. Tarn, M. Xue, X. Wang, S. Lin, Z. Ji, R. Li, F. L. Garcia, J. Yang, M. L. Kirk, T. Xia, J. I. Zink, A. Nel and C. J. Brinker, *J. Am. Chem. Soc.*, 2012, **134**, 15790–15804.
29 M. van der Zande, R. J. Vandebriel, M. J. Groot, E. Kramer, Z. E. Herrera Rivera, K. Rasmussen, J. S. Ossenkoppele, P. Tromp, E. R. Gremmer, R. J. B. Peters, P. J. Hendriksen, H. J. P. Marvin, R. L. A. P. Hoogenboom, A. A. C. M. Peijnenburg and H. Bouwmeester, *Part. Fibre Toxicol.*, 2014, **11**, 8.
30 A. D. Maynard, *Nat. Nanotechnol.*, 2014, **9**, 658–659.
31 M. Kosmulski, J. Hartikainen, E. Mączka, J. Władysław and J. B. Rosenholm, *Anal. Chem.*, 2002, **74**, 253–256.
32 Z. Xu and M. Cotlet, *Angew. Chem., Int. Ed.*, 2011, **50**, 6079–6083.
33 C. Tanielian, C. Wolff and M. Esch, *J. Phys. Chem.*, 1996, **100**, 6555–6560.
34 J. Liu, C. Detrembleur, S. Mornet, C. Jérôme and E. Duguet, *J. Mater. Chem. B*, 2015, **3**, 6117–6147.
35 T. E. Decoursey, *Physiol. Rev.*, 2003, **83**, 475–579.
36 R. Lawaczeck, *Berichte der Bunsengesellschaft für physikalische Chemie*, 1988, **92**, 961–963.

37 A. C. Marques, P. J. Costa, S. Velho and M. H. Amaral, *J. Controlled Release*, 2020, **320**, 180–200.
38 V. Tokárová, A. Pittermannová, V. Král, P. Řezáčová and F. Štěpánek, *Nanoscale*, 2013, **5**, 11490–11498.
39 J. B. Verlhac, A. Gaudemer and I. Kraljic, *Nouv. J. Chim.*, 1984, **8**, 401–406.
40 M. A. Rubio, D. O. Mártire, S. E. Braslavsky and E. A. Lissi, *J. Photochem. Photobiol., A*, 1992, **66**, 153–157.
41 R. D. Hall and C. F. Chignell, *Photochem. Photobiol.*, 1987, **45**, 459–464.
42 B. A. Lindig, M. A. J. Rodgers and A. P. Schaap, *J. Am. Chem. Soc.*, 1980, **102**, 5590–5593.
43 H.-R. Choi Kim, Y. Luo, G. Li and D. Kessel, *Cancer Res.*, 1999, **59**, 3429–3432.
44 R. Mandelkow, D. Gumbel, H. Ahrend, A. Kaul, U. Zimmermann, M. Burchardt and M. B. Stope, *Anticancer Res.*, 2017, **37**, 2239–2244.